analytical chemistry

Article

Optimization of a Paper-Based ELISA for a Human Performance Biomarker

Richard C Murdock, Li Shen, Daniel K Griffin, Nancy Kelley-Loughnane, Ian Papautsky, and Joshua Andrew Hagen

Anal. Chem., **Just Accepted Manuscript** • Publication Date (Web): 11 Nov 2013

Downloaded from http://pubs.acs.org on November 12, 2013

Report Documentation Page

Form Approved
OMB No. 0704-0188

1. REPORT DATE	2. REPORT TYPE	3. DATES COVERED
11 NOV 2013		**00-00-2013 to 00-00-2013**

4. TITLE AND SUBTITLE	5a. CONTRACT NUMBER
Optimization of a Paper-Based ELISA for a Human Performance Biomarker	5b. GRANT NUMBER
	5c. PROGRAM ELEMENT NUMBER
6. AUTHOR(S)	5d. PROJECT NUMBER
	5e. TASK NUMBER
	5f. WORK UNIT NUMBER
7. PERFORMING ORGANIZATION NAME(S) AND ADDRESS(ES) **711 HPW/RHXBC, Human Signatures Branch,Human Effectiveness Directorate, 711th Human,Performance Wing,Wright-Patterson Air Force Base,OH,45433**	8. PERFORMING ORGANIZATION REPORT NUMBER
9. SPONSORING/MONITORING AGENCY NAME(S) AND ADDRESS(ES)	10. SPONSOR/MONITOR'S ACRONYM(S)
	11. SPONSOR/MONITOR'S REPORT NUMBER(S)

12. DISTRIBUTION/AVAILABILITY STATEMENT
Approved for public release; distribution unlimited

13. SUPPLEMENTARY NOTES

14. ABSTRACT

15. SUBJECT TERMS

16. SECURITY CLASSIFICATION OF:			17. LIMITATION OF ABSTRACT	18. NUMBER OF PAGES	19a. NAME OF RESPONSIBLE PERSON
a. REPORT **unclassified**	b. ABSTRACT **unclassified**	c. THIS PAGE **unclassified**	**Same as Report (SAR)**	**33**	

Optimization of a Paper-Based ELISA for a Human Performance Biomarker

Richard C. Murdock[1,2], Li Shen[2], Daniel K. Griffin[2], Nancy Kelley-Loughnane[1], Ian Papautsky[2*], and Joshua A. Hagen[1*]

[1]*711 HPW/RHXBC, Human Signatures Branch, Human Effectiveness Directorate, 711th Human Performance Wing, Wright-Patterson AFB, OH, USA.*

[2]*BioMicroSystems Lab, School of Electronic and Computing Systems, University of Cincinnati, Cincinnati, OH, USA.*

Abstract

Monitoring aspects of human performance during various activities has recently become a highly investigated research area. Many new commercial products are available now to monitor human physical activity or responses while performing activities ranging from playing sports, to driving, and even sleeping. However, monitoring cognitive performance biomarkers, such as neuropeptides, is still an emerging field due to the complicated sample collection and processing, as well as the need for a clinical lab to perform analysis. Enzyme-linked immunosorbent assays (ELISAs) provide specific detection of biomolecules with high sensitivity (pM concentrations). Even with the advantage of high sensitivity, most ELISAs need to be performed in a laboratory setting and require around six hours to complete. Transitioning this assay to a platform where it reduces cost, shortens assay time, and is able to be performed outside a lab is invaluable. Recently developed paper diagnostics provide an inexpensive platform to perform ELISAs on; however, the major limiting factor for moving out of the laboratory environment is the measurement and analysis instrumentation. Using something as simple as a digital camera or camera-enabled Windows- or Android-based tablets, we are able to

image a paper-based ELISAs (P-ELISAs), perform image analysis, and produce response curves with high correlation to target biomolecule concentration in the 10 pM range. Neuropeptide Y detection was performed Additionally, silver enhancement of Au NPs conjugated with IgG antibodies showed concentration dependent response to IgG; thus, eliminating the need for an enzyme-substrate system. Automated image analysis and quantification of antigen concentrations are able to be performed on Windows- and Android-based mobile platforms.

Introduction

The idea of monitoring human performance through biomarkers has recently become a highlighted topic in many fields. Assessing cognitive state, physiological state, and/or stress levels is of concern in a wide range of professions, including air traffic control settings[1], anesthesiologists[2,3], professional athletes[4], commercial aviation pilots[5,6], military unmanned combat aerial vehicles (UCAV) pilots[7], and ground troops[8]. One of the predominant biomarkers of interest is Neuropeptide Y (NPY) due to its association with the regulation of stress and anxiety[9,10], fear, learning and memory[11,12], blood pressure[13,14], food intake[15], and sympathetic nervous system activity[16]. These markers are very relevant for diagnoses and treatment of post-traumatic stress disorder (PTSD)[17], which is of significant interest for returning deployed military personnel. Also, they are very relevant to military occupations which require high vigilance over long periods of time and the ability to adapt in a stressful environment. NPY is the most abundant neuropeptide in the human brain[18], with high levels of expression in the amygdala, hypothalamus, cortex, and hippocampus[18], and is widely expressed throughout the central nervous system[18-20]. The role of NPY in the behavioral effects of stress in humans has

been explored by studies where the plasma NPY concentrations of soldiers undergoing military survival training were measured following extreme interrogation stress[8]. High NPY levels were indicative of individuals with more stress resilience, or "stress hardiness", and had better performance scores, whereas lower NPY was related to symptoms of dissociation[8]. Additionally, when comparing a group of special forces troops to a group of general troops after exposure to uncontrollable stress, the special forces troops had a higher average change of NPY levels between baseline and stressed states, indicating that NPY could help with "stress toughness"[21]. NPY levels have also been shown to increase significantly after a traumatic brain injury (TBI) event[22]. The ability to quickly and inexpensively assess levels of NPY could provide significant advantages in the early determination of personnel stress levels in mission-critical roles, early TBI diagnoses, as well as diagnoses and treatment of PTSD.

Paper microfluidic analytical devices have emerged in recent years[23,24], leading to development of a number of point-of-care (POC) analyses, including HIV chips[25,26], paper-based ELISA[27-29], and low-cost colorimetric diagnostic assays[30-35]. A paper-based enzyme-linked immunosorbent assay (P-ELISA) combines the sensitivity and specificity of an ELISA with the convenience, low cost, and ease-of-use of paper-based platforms[27]. P-ELISAs are much faster to complete, with results in under an hour, whereas conventional ELISAs would require a minimum of 6 hours to complete. Costs are significantly reduced as well, since only 3 μL each of sample, blocking, antibody, and substrate solutions are needed for each test zone. This means that ~17 P-ELISA plates could be performed from one 96-well plate conventional ELISA kit, assuming the amount of secondary (or enzyme-labeled) antibody is the limiting factor. Another significant advantage of using paper microzone plates is that it allows the user to print plates "on-demand" and opens opportunities for a wide range of non-standard formats for customized assays[36].

Colorimetric results of these assays can be viewed by naked eye, although it is difficult to precisely quantify the small changes in the analyte amount[37]. Promising colorimetric detection results have been demonstrated using video cameras[38], digital color analyzers[39], scanners[40] or custom portable readers[31]. Here we demonstrate the use of a digital camera to image the P-ELISA for detection of rabbit IgG, and use color-based image processing techniques to quantify substrate concentration changes. This technique not only allows for a wider range of colorimetric substrates to be used since it does not limit the imaging dynamic range through conversion to grayscale, it also means that a mobile-device camera could be used to perform measurements outside a laboratory setting. A key drawback of all these methods is the need for specialized instrumentation and for manual image analysis with a computer. Image measurement automation was achieved using MATLAB, for a Windows-based tablet, and an Android-based app (.APK) for an Android-based tablet.

To verify operation of the P-ELISA, we performed a standard 96-well plate-based ELISA procedure on the P-ELISA platform for detection of rabbit IgG with a colorimetric substrate. We used a wax-printed 96-microzone paper plate with a 12x8 array of circular test zones for running multiple P-ELISAs in parallel. This allowed us to use common microplate processing techniques with the P-ELISA format. For our wax-printed microzone plates, each test zone was 3 mm in diameter and required a minimum of 1.5 μL of solution to completely wet the test zone; however, 3 μL of solution were used to provide ample wetting without over-saturation. As reported in Cheng et al., smaller test zones could be used in this format with similar test results, but were kept in a 96-well similar configuration for ease of laboratory processing and imaging[27]. Additionally, we performed optimization tests for detection of IgG and NPY with different

enzymes and enzyme substrates for use with the P-ELISA platform. We also examined the effect of physiological sample solutions on the P-ELISA operation and assay sensitivity.

Materials

Chemicals/Solutions required:

Rabbit IgG (1 mg/mL), goat anti-rabbit IgG antibody conjugated with Alkaline Phosphatase (AP) enzyme (1 mg/mL), goat anti-rabbit IgG antibody, and the *p*-Nitrophenyl Phosphate (pNPP) substrate for ELISA were purchased from Sigma Aldrich. Neuropeptide Y (NPY) was purchased from GenScript. Mouse anti-human Neuropeptide Y monoclonal antibody, 1-Step Ultra TMB-ELISA, SuperSignal ELISA Pico Chemiluminescent Substrate, and the QuantaBlu Fluorogenic Peroxidase Substrate Kit were purchased from Thermo-Pierce. The AP and horseradish peroxidase (HRP) Lightning Link Enzyme Labeling Kits were purchased from Innova Biosciences. The thiol- and carboxyl-modified poly(ethylene glycol) (PEG) was purchased from Prochimia. The blocking buffer consisted of 0.05% v/v Tween 20 and 1% w/v bovine serum albumin in 1X phosphate-buffered saline (PBS). The antibody incubation solution contained 0.05% v/v Tween 20 in 1X PBS with the conjugated antibody (1:1000 ratio). The NBT/BCIP colorimetric substrate consisted of 2.68 mM 5-bromo-4-chloro-3-indolylphosphate toluidine salt (BCIP), 1.8 mM nitro-blue tetrazolium chloride (NBT), 5 mM $MgCl_2$, 100 mM NaCl, and 0.05% v/v Tween 20 in 100 mM Tris Buffer (pH 9.5). Unfiltered human saliva was obtained from Innovative Research.

Methods

Printing of Paper 96-well Plates

A 'negative' image of a 96-well plate was designed using MS PowerPoint (or any computer-aided drawing program) where wax occupies the areas between wells and the inside of the wells are empty. The outside plate dimensions and well spacing were matched to a standard Costar 96-well microtiter plate. The printed well diameters prior to melting were ~5.56 mm, which was reduced from a normal well diameter to provide the optimal bed volume in each well after melting. Using a Xerox ColorQube 8570N solid wax ink printer, a wax image of the 96-well plate was printed onto Whatman #1 filter paper by attaching the filter paper to an 8.5"x11" sheet of paper for proper printer feeding. After allowing cooling for about 10 seconds, the filter paper was placed onto a hot plate (#3 setting) to allow the wax to fully melt through the wax paper evenly across the entire plate (~4 minutes). Plate was allowed to cool fully and could then be used immediately or stored for later use. Final well diameters after melting were ~3.8 mm.

Paper-Based ELISA

After creating the 96-well plate via the wax printing method, the plate was placed on a pipette tip box with the open side up. Initially, 3 µL of target solution was added at the desired concentration to each well (min 3 wells each). This was incubated at room temperature for 10 minutes and then each well was blocked with 3 µL of blocking buffer. Following an additional 10 minute incubation period, 3 µL of antibody incubation solution was added to each sample well and incubated for 2 minutes. Each well was then washed two times with 10 µL of 1X PBS while wicking away any excess solution in between washes with blotting paper. Finally, 3 µL of the enzymatic substrate was added to each well and allowed to incubate at room temperature for

the appropriate period of time. For the BCIP/NBT, pNPP, and TMB substrates, the incubation was allowed to continue until the samples dried completely (~30 min), and then the samples were imaged. The chemiluminescent substrate was incubated for 2 min and then imaging was performed due to the assay intensity degrading after 5 min. All assays were repeated in triplicate or quadruplicate.

Enzyme-free P-ELISA

Gold nanoparticles (Au NPs) with an average diameter of 16 nm were synthesized through previously published citrate-reduction techniques[41-44]. The Au NPs (3 mL, 10 nM, Millipore water) were then conjugated with poly(ethylene glycol) (PEG) (20 μL, 1mM) which contained a thiol group on one end and a carboxylic group on the other end. The mixtures were left in the dark overnight to allow for chemisorption of the thiol groups onto the surface of the Au NPs. The particles were washed multiple times via centrifugation with subsequent buffer exchanges to remove any unbound PEG molecules. Anti-rabbit IgG antibodies were then conjugated to the carboxylic end of the PEG through EDC/NHS (N-(3-Dimethylaminopropyl)-N′-ethylcarbodiimide hydrochloride/N-Hydroxysuccinimide) linkage chemistry. Briefly, freshly prepared EDC (30 μL, 20 nM) and NHS (10 μL of 50 nM) were added to the Au NP-PEG-COOH (30 μL, 10 nM) solution containing MES buffer (30 μL, pH 5.5) and mixed for 30 min. Phosphate buffered saline (PBS) (250 μL, 1X, pH 7.55) was then added to the solution as well as 1.1 μL of the anti-rabbit IgG antibody stock. After mixing for 30 min, the particles were washed multiple times via centrifugation with subsequent buffer exchanges, with a final resuspension volume of 100 μL.

The P-ELISA was carried out as described earlier, with 3 μL of the Au NP-IgG Ab solution replacing the conventional antibody step. Development was performed through a silver enhancement staining kit (Ted Pella / BBInternational) where 3 drops of both the initiator and enhancer were mixed together and then 3 μL of the solution was applied to each test zone and allowed to develop until dry.

Image analysis methods

Images were captured primarily using a Canon EPS/Rebel T3i/EOS 600D camera; however, for the comparison of different imaging methods, an HTC Droid Eris smartphone and an HP Color 4540 Scanner/Printer were used as well.

For manual processing of the P-ELISAs, the image captured by the camera was opened using ImageJ (NIH). An average RGB value was obtained for each test spot by selecting the test spot area, excluding the transition from color to gray-black wax at the edges, and then selecting the color histogram function in ImageJ. These average RGB values were then transferred into an Excel workbook which calculated the ΔRGB (Eq. 1) values relative to the control well values and also converted each value into the corresponding CIE 1931 color space coordinates (and ΔCIE) as described in our previous paper[46]. The ΔRGB calculation (Eq. 1) determines the magnitude of the vector between the original (control) RGB value (R_0,G_0,B_0) and the RGB value of interest (R_n,G_n,B_n). This was, at minimum, repeated in triplicate for each concentration of antigen tested. Since all assays attempted use a single color shift (i.e. clear to purple, clear to yellow, etc.), the ΔRGB values provided more consistent correlation to antigen concentration than the ΔCIE values. However, if the assays had a two color shift (i.e. blue to green, or clear to yellow to red), the ΔCIE values would be necessary to use for correlation as the ΔRGB values

would cause poor correlation due to the potential for overlapping values for different concentrations of sample. The ΔRGB values were plotted against antigen concentration to obtain a semi-log or log-log best fit equation using GraphPad Prism. Sensitivity and limit-of detection values were determined by the 3σ method and by comparison of the 3σ value to the background or control values.

$$\Delta\text{RGB} = \sqrt{(R_n - R_0)^2 + (G_n - G_0)^2 + (B_n - B_0)^2}$$

Equation 1. Delta RGB (ΔRGB) Calculation.

For automated image processing, image processing code was written into an M-file for execution by MATLAB R2011a (The Mathworks, Inc.) which include the Image Processing Toolbox. The code prompts the user to select an image to open from file which is then converted into a 3-D array with red, green, and blue channel data in different layers. Next, a grey level threshold is determined automatically for the image and is used to convert the RGB image to a black and white (BW) image. Once converted, the program identifies the circular test zones, which are now white spots, by excluding white spots with an eccentricity greater than 0.5 and/or an area of less than 1000 pixels. This defines a mask for the original image, but since we want to exclude the edges of the white areas to prevent averaging any gray/black values into our RGB values, the white spot areas are reduced by 50% while maintaining the centroid position for each. The final mask is then applied to the original image where the average RGB intensity values are obtained for each circular area in the mask. The ΔRGB values are calculated from this data and concentrations are estimated by solving the semi-log best fit (log x, y) equation. Finally, the centroids and the concentrations for each area are output for display on the original image.

Additionally, the average red, green, and blue channel values and corresponding calculated concentration for each well are output in an Excel spreadsheet (.xls).

The android application (.APK) implementation of the colorimetric algorithm is similar to the automated image processing MATLAB solution. Once an image is selected to analyze, either from device storage or captured from within the application, a calibration curve can be created. During calibration, the user selects a series of control tests at increasing concentrations of target and then assigns numeric concentration values to them. The app determines the "color" of each selection using an incremental average of the red, green, and blue pixel values from within the selection area on the screen. After the calibration is finished, the app converts all test spot RGB values to ΔRGB values (Eq. 1), along with a zero calibration point with an assigned concentration of 0. A regression is then created based on the equation: $\log(y) = b * \log(x) + a$, since a log-log response was observed for the pNPP substrate. The user can now return to the image of interest and begin selecting unknown test areas to analyze. For each unknown test area selected, the app calculates the average RGB, converts to ΔRGB values, and the corresponding concentration can be determined using the regression equation. The app also stores all data into a text file which can be transferred via email attachment or Bluetooth file transfer to perform further data analysis.

Results and Discussion

Optimization of P-ELISA for NPY Detection

We began with verifying the P-ELISA operation on wax-printed Whatman filter paper using the colorimetric substrate (BCIP/NBT) and AP-labeled anti-rabbit IgG antibodies. We

were able to measure rabbit IgG over a range of 0.1 to 5 μM using the ΔRGB image analysis method (Figure 1A), which allowed us to not only verify the P-ELISA procedure, but to confirm the ability to use the ΔRGB method of analysis against the black-and-white image conversion method used in Cheng et al. with similar antigen concentration ranges[27].

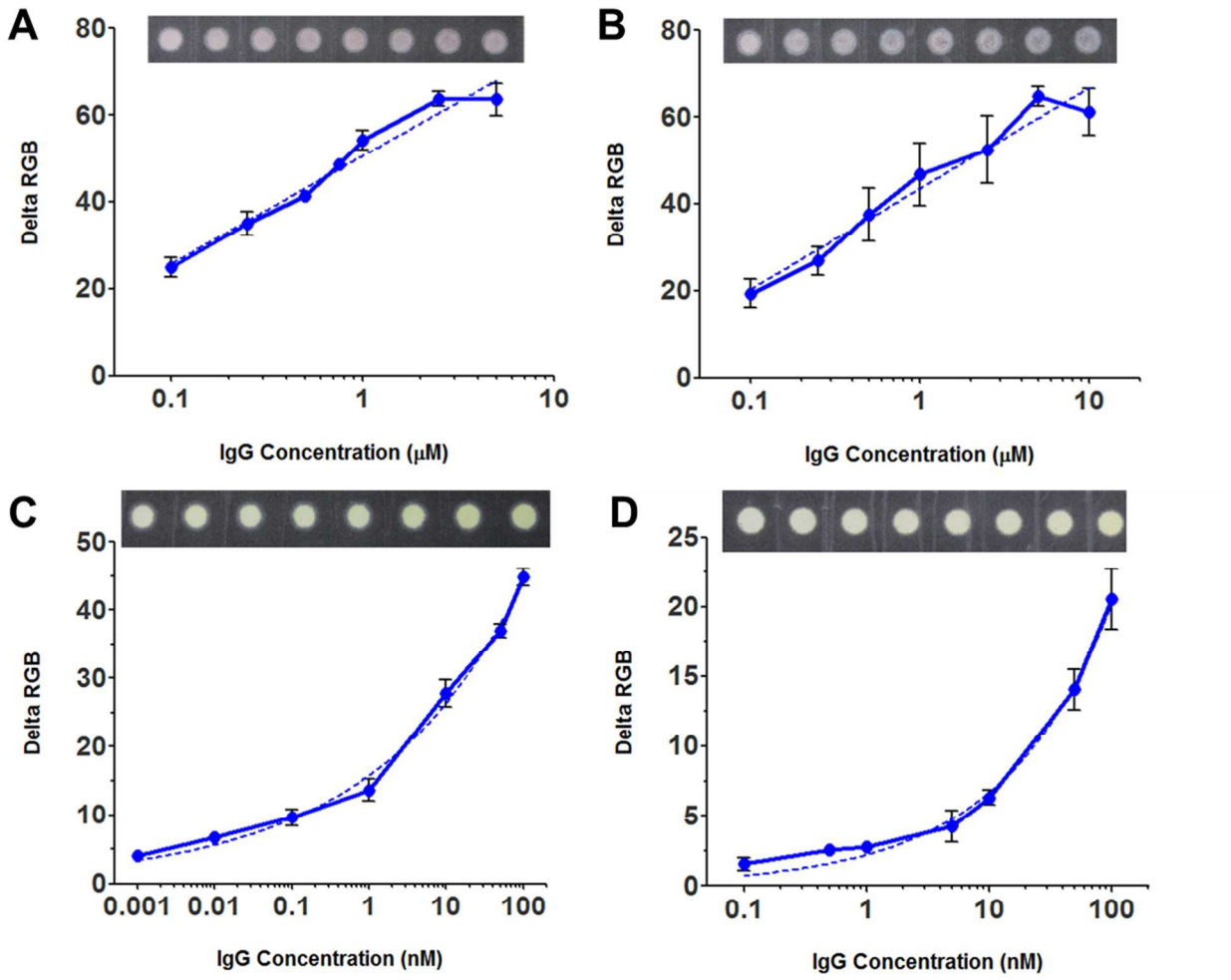

Figure 1. Effect of Enzyme Substrates and Sample Media Complexity on P-ELISA Function. (A) Rabbit IgG in DI H_2O using BCIP/NBT Substrate with a semi-log best fit (log x, y). (B) Rabbit IgG in human saliva using BCIP/NBT substrate with a semi-log best fit (log x, y). (C) Rabbit IgG in DI H_2O using pNPP Substrate with a log-log best fit (log x, log y). (D) Rabbit

IgG in human saliva using pNPP Substrate with a log-log best fit (log x, log y). Error bars indicate standard error of the mean (SEM) with n=4.

We then evaluated a different substrate with our P-ELISA to assess compatibility with the paper platform and any changes to the sensitivity, or LOD, of the assay. A common colorimetric substrate that is used in ELISAs in conjunction with the AP enzyme is p-nitrophenyl phosphate (pNPP). This substrate produces a clear to yellow color change in liquid as enzyme concentration increases and the change in absorption is monitored at 405 nm using a spectrophotometer. However, using a digital image and our image analysis process, we are able to track this change in color intensity through ΔRGB calculations. By not having to convert the image to grayscale, this allows a greater dynamic range of measurement with increased sensitivity, which is discussed in the image analysis optimization section. Even though it may be hard to visually identify minute differences between consecutive samples, we can visually detect the overall trend of increasing substrate conversion with increasing IgG concentration (Figure 1).

Once the color image processing is applied, the relationship can be easily quantified via ΔRGB. While both substrates provide responses to increasing concentrations of IgG, the pNPP substrate provided significant improvement in the limit of detection of the assay (Figure 1C). We did find it interesting that the NBT/BCIP substrate produces a logarithmic response curve, while the pNPP substrate produces a linear response. Using the 3σ of the lowest concentration sample, we determined the limit of detection (LOD) of IgG with the pNPP substrate to be 7.5 pM (Figure 1C). This is 4 orders of magnitude improvement over what was reported in Cheng et al. where the lowest IgG concentration attempted was 670 nM, which was lower than their reported LOD[27]. The conversion of the BCIP/NBT substrate is a two-step process, with the BCIP being

directly hydrolyzed by the alkaline phosphatase enzyme and then the intermediate "indoxyl" product dimerizes with the NBT, reducing it to form the insoluble NBT-formazan indigo-colored dye. In contrast, the pNPP substrate is a one-step, direct hydrolysis of the pNPP to a soluble yellow end-product, p-nitrophenol. We suspect that the significant increase in sensitivity of the assay using the pNPP substrate is due primarily to the BCIP/NBT system relying on this two-step process, with the paper matrix potentially limiting the diffusion of the products and hindering the efficiency of the NBT to NBT-formazan conversion. It is also possible that the alkaline phosphatase enzyme exhibits differences in the rate of hydrolysis between the pNPP and BCIP substrates.

We compared the effects of sample media complexity on the performance of the P-ELISA by spiking similar concentrations of IgG into unfiltered human saliva. We tested the effect on the P-ELISA results using both the NBT/BCIP and pNPP substrates (Figures 1B and 1D). Variability increased between replicate samples for the NBT/BCIP substrate, with the LOD increasing to 250 nM from 160 nM without saliva. The saliva caused the pNPP substrate LOD to increase as well (1.72 nM), but sample-to-sample reproducibility was much better. Even though sensitivity is reduced from using a more purified sample, it was thought that using a more complex media would significantly hinder the assays function, even to the point of completely debilitating the P-ELISA. However, this does not appear to be the case, which provides a promising outlook for moving forward with paper-based diagnostics with more complex biological samples.

Our goal was to use the P-ELISA format to detect Neuropeptide Y, a human performance biomarker that indicates stress levels and potentially cognitive state. After conjugating the anti-human NPY antibody with the AP, the P-ELISA was performed with both

the NBT/BCIP and pNPP enzyme substrates (Figure 2). While both substrates produced similar LODs, ~2.3 nM for NBT/BCIP and ~4.0 nM for pNPP, the replicate sample variability was significantly reduced for the pNPP substrate, as seen previously with the IgG experiments (Figure 2B). The tendency for the pNPP substrate to produce a log-log response curve was also observed with the NPY sample (Figure 2B). While the choice of enzyme substrate for the NPY P-ELISA does not appear to have a significant impact on the LOD, as observed in the rabbit IgG P-ELISA, the limiting factor here may not be the substrate itself. Multiple other factors could be affecting the LOD, such as antibody-enzyme labeling efficiency, anti-NPY affinity for NPY, and the accessibility of anti-NPY to bind NPY on the paper matrix due to the small size of NPY. Additionally, since plasma NPY concentrations can range from ~50-100 pM for non-stressed, healthy individuals[8,21,45] to ~400-1400 pM for individuals experiencing acute stress[8,21], further optimization of the NPY P-ELISA is needed to extend the LOD into the pM range by addressing the factors listed previously.

For NPY in human saliva, we observed a similar decrease in LOD (~30 nM) as with IgG when compared to NPY dispersions in DI H_2O and sample-to-sample variability was unaffected (Figure 2C). The unfiltered saliva was primarily used as a mimic for a more complex biological fluid in this study; however, NPY has been found in salivary samples of resting subjects at ranges of 3.3 to 15.2 pM[45]. Even though this is an order of magnitude lower concentration than plasma NPY, it could provide a less intrusive method for the detection of cognitive biomarkers.

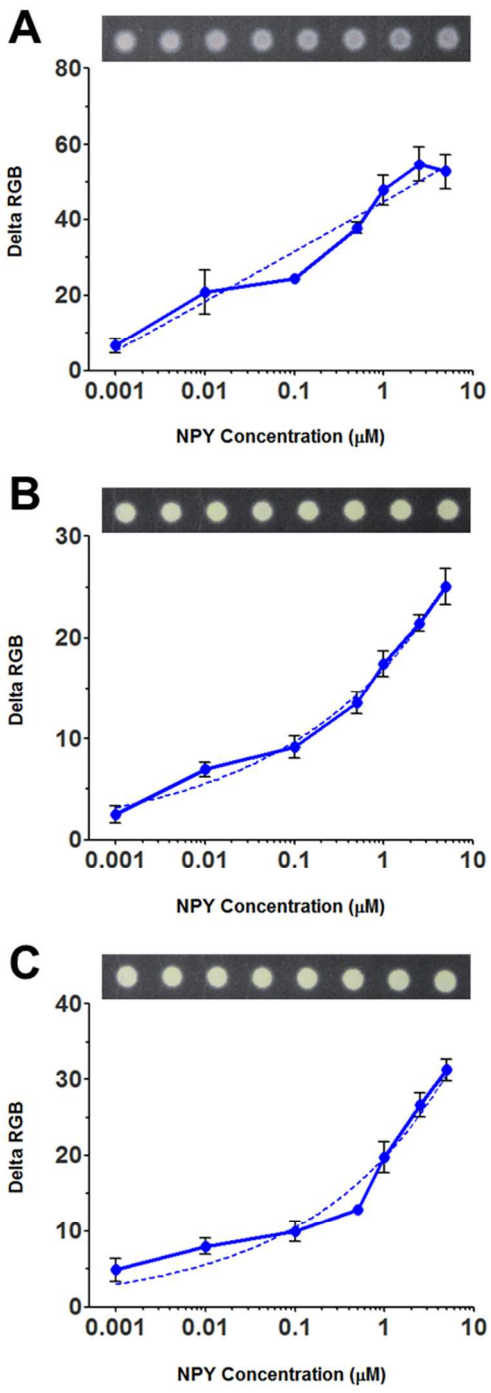

Figure 2. Comparison of Enzyme Substrates and Media Complexity for the Detection of NPY using P-ELISA. (A) Detection of NPY using BCIP/NBT substrate. (B) Detection of NPY

using pNPP substrate. (C) Detection of NPY in human saliva using pNPP substrate. Error bars indicate SEM with n=4.

In addition to comparing two different enzyme substrates for the AP enzyme, we also tested substrates with the horseradish peroxidase conjugated NPY antibody to compare any detection limit or sensitivity enhancements/degradation. In a normal 96-well ELISA, HRP enzyme-labeled antibodies provide increased sensitivity due to higher reduction of their appropriate substrates per molecule of HRP compared to AP, and are compatible with a wider range of chemiluminescent and fluorometric substrates as well. HRP also has significant size advantage over AP, ~44 kDa for HRP and ~140 kDa for AP, which allows for quicker diffusion and higher enzyme to antibody ratios. Although the enzymes do require different colorimetric substrates, which complicate direct comparison of the enzyme functionalities on paper, both substrates are one-step solutions to minimize processing variation.

We found that the TMB colorimetric substrate showed significantly reduced sensitivity of NPY (Figure 3). The LOD was reduced two orders of magnitude to ~0.5 μM. Similarly, the performance of the chemiluminescent substrate, which was imaged ~2 minutes after the addition of the substrate, was very poor and produced erratic results (Supplemental Figure 1). There does appear to be a general trend of increasing luminescence with increasing concentration; however, the sample-to-sample reproducibility had high variation. The most likely reason for this is that the paper substrate is interfering not only with the function of the HRP enzyme, but also with the diffusion of the chemiluminescent substrate through the paper therefore limiting the ability of the HRP enzyme to reduce the substrate. Wang et al. demonstrated a similar chemiluminescent

assay with a chitosan-modified paper substrate, which appears to stabilize the response of the assay through minimizing the interaction of the antigen with the cellulose fibers[28]. However, the chemiluminescent assay used in that study was based on a sandwich ELISA, with capture antibodies on the surface of the paper substrate, which could further reduce any unwanted interactions, but also increases cost and complexity of the assay.

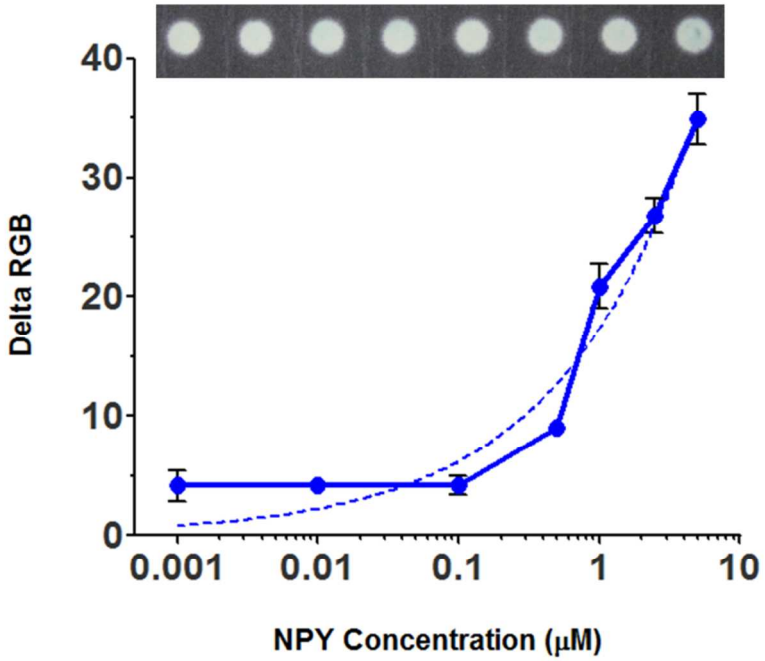

Figure 3. P-ELISA of NPY in DI H_2O using HRP-labeled NPY Antibody and Colorimetric Substrate. Semi-log best fit (log x, y). Error bars indicate SEM with n=4.

One goal of the P-ELISA is to move this procedure out of the normal laboratory environment. A step toward achieving this would be to eliminate the enzyme altogether to have less stringent storage conditions of reagents and increase their longevity. Proteins are susceptible to degradation in solution during long-term storage at room temperature or at 4 °C primarily due

to proteases, microbial contamination, or oxidation. Enzymatic activity is more likely to be degraded before antibody activity, due to their mostly globular structure, since any slight change in their conformation would more severely impact the enzyme's function. Additionally, antibody (Ab) conjugation with gold nanoparticles (AuNPs) has been used quite extensively in lateral flow assay (LFA) applications where the Ab-AuNP conjugates are lyophilized on the devices with minimal decreases in Ab activity. This could provide a long-term storage solution where the Ab-AuNP conjugates could be resuspended when ready to be used. In place of an enzyme substrate, we chose to use a silver enhancement method where the Ag^{+} are precipitated onto the surface of the AuNPs and provide the same sort of signal amplification that the enzyme-enzyme substrate provides (Figure 4b). We found this technique to have very good sample-to-sample reproducibility and exhibit a high correlation coefficient to a log-log type response (Figure 4a). LOD for IgG with IgG Ab-AuNPs was ~10 nM using the silver enhancement reporter method. While this method does fall short of the LOD when using antibody-enzyme conjugates, it does provide an alternative method for signal amplification which would be more robust for long-term storage conditions.

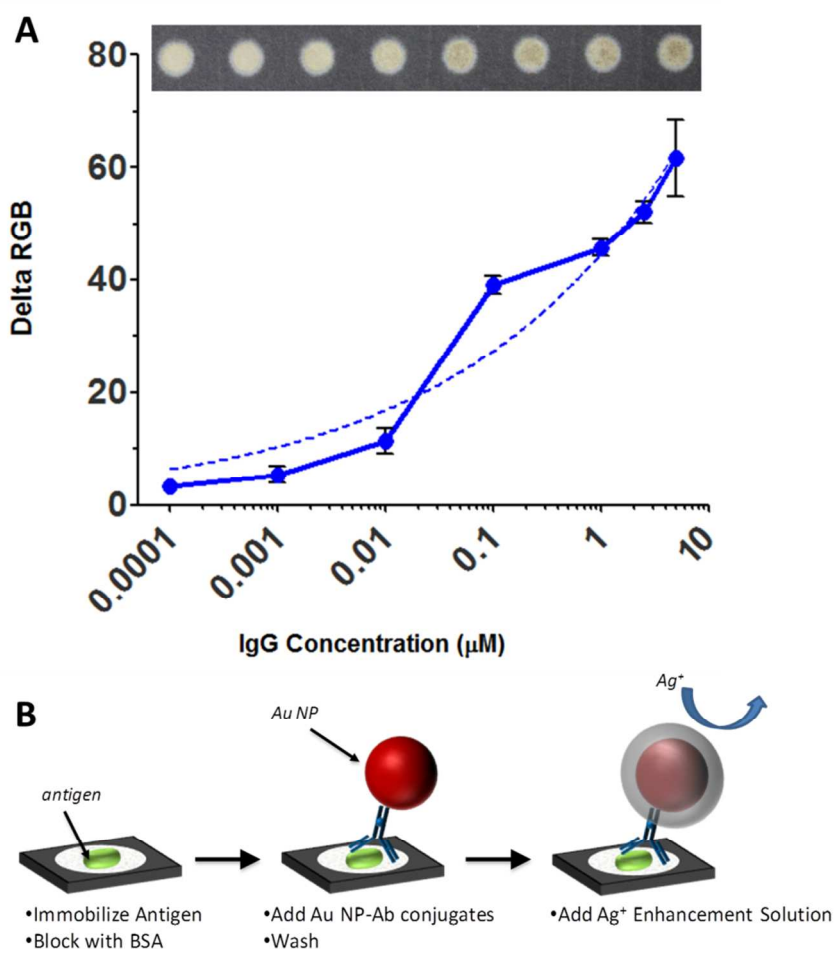

Figure 4. Enzyme-free P-ELISA of Rabbit IgG in DI H_2O using IgG antibody conjugated Au NPs with silver enhancement stain. (A) Plot of delta RGB vs. IgG concentration using Au NP – silver enhancement procedure. Error bars indicate SEM with n=4. (B) Schematic of Enzyme-free P-ELISA Assay.

Optimization of Image Analysis

A common method for analyzing color images is to first convert the RGB image to a grayscale image, thereby simplifying analysis since each pixel corresponds to an intensity value. This

works well for any sample where the color shift provides an increasingly opaque substance so that, when converted to a grayscale image, the pixel intensity values can be observed to decrease with increasing opacity. This was shown in Cheng et al., where the enzyme substrate chosen produced an increasingly darker blue/purple color with increasing amounts of antibody-enzyme conjugates and therefore antigen as well. However, since we found the pNPP substrate to have better sample-to-sample consistency, increased sensitivity, and nearly identical limits-of-detection, we determined that this grayscale conversion would significantly limit the measurement sensitivity.

To demonstrate this issue, we used a CMYK standard printer calibration scale which contained yellow and white-black scale standards (Supplemental Figure 2). An image was taken of the calibration scales and the same image analysis process was performed as for the P-ELISA. The color image of the scales were analyzed using the ΔRGB method and then the image was converted to grayscale and analyzed by pixel intensity values since ΔRGB method is not possible. The white-black scale was assumed to be the "maximum" change possible in both conditions (i.e. 0 to 100 on the white-black scale is 0 to 100%). This allowed us to compare the change in response range of the yellow-scale for the color and grayscale images (Figure 5).

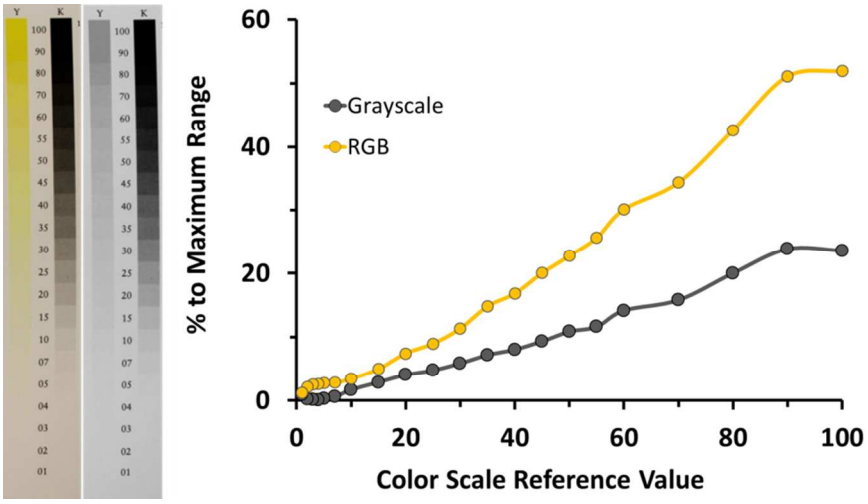

Figure 5. Comparison measurement of simulated pNPP ELISA substrate using delta RGB or grayscale analysis. (Left image) Color image of simulated yellow substrate scale and white-black scale. (Right image) Image after grayscale conversion. Plot shows the comparison of the yellow scale (simulated substrate) to the white-black scale as a percentage of maximum value in both the RGB and Grayscale images.

Even though the identical image was used for both analyses, a 30% reduction can be seen in the available response range when the image is converted to grayscale. This in turn leads to decreased measurement sensitivity since a larger antigen concentration shift is required to measure the same intensity shift. For example, in Figure 5, to measure the same percentage shift from 20 to 40 color units on the RGB plot, it would require a change of 35 to 75 color units on the grayscale plot which equates to roughly a 50% decrease in sensitivity.

Additionally, we tested the method of image capture to observe and quantify its effect on the measurement response range. We imaged the same P-ELISA using 3 different methods: a DSLR camera, a smartphone camera, and an RGB flatbed scanner (Figure 6). We found that the

flatbed scanner and smartphone camera provided similar response ranges and slopes, while the DSLR camera provided the largest range and highest slope which indicates better measurement sensitivity (Figure 6). All images in this manuscript which were used for analysis were captured using the DSLR camera.

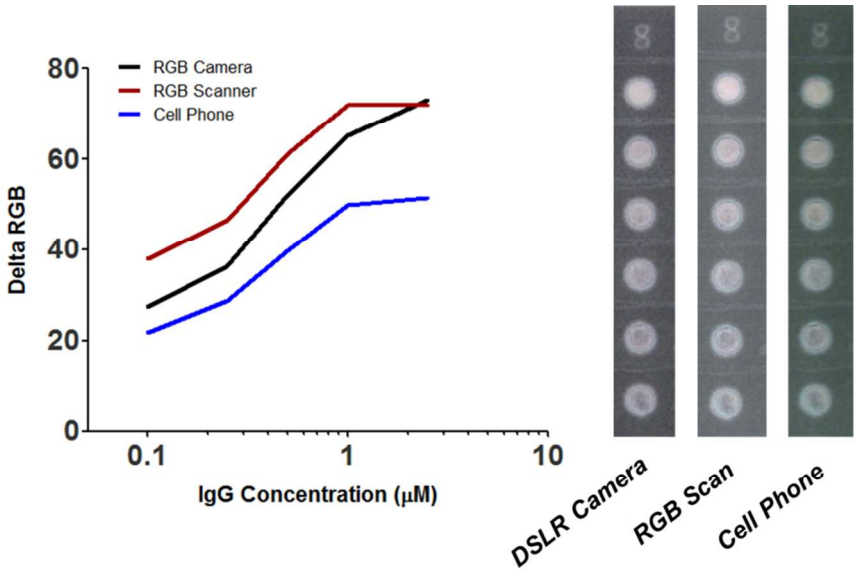

Figure 6. Comparison of P-ELISA Imaging Methods and the Effect on Measurement Sensitivity Range. Plot shows comparison of the measured delta RGB of the same sample via DSLR camera, RGB scanner, and smartphone camera. Visual comparison of the digital images shows minor color variations between the three imaging methods.

As our group has previously reported[46], the CIE coordinate system can provide a better method of tracking color changes in an image than purely basing the response from either of the red, green, or blue channels. Interestingly, when we attempted to use the ΔCIE method for

image analysis, which normally correlates color changes very efficiently, the results were not as accurate as the ΔRGB method. The ΔCIE method works excellently for assays which produce a wide range of color responses, such as pH testing; however, when applied to the P-ELISA method, which is a single color intensity shift, measuring the change in RGB values provides a more consistent correlation to changes in antigen concentration than using the changes in the CIE coordinates. Even when analyzing the same sample, the two methods produce quite different correlation curves when plotted against antigen concentration (Figure 7). We concluded that since the output of the P-ELISA assay is primarily an intensity change of the same color, the ΔRGB method is more appropriate in this instance.

Manually processing each test zone through ImageJ and Excel, as performed for the experiments in this work, is extremely tedious and time-consuming, and the process could be difficult to train new people how to use. Additionally, with the idea that P-ELISAs could be performed within a resource limited laboratory, we developed an automated image analysis program using MATLAB. Here, the user takes an image using a tablet capable of running MATLAB (in this case a Fujitsu Windows-based Tablet) and then runs the program (m-file) in MATLAB (Figure 8A). The user is prompted to select the image to analyze and the program automatically identifies the test zones on the paper-based 96-well microplate. The output of the program is a visual image of the analyzed plate with the corresponding calculated concentrations for each test zone.

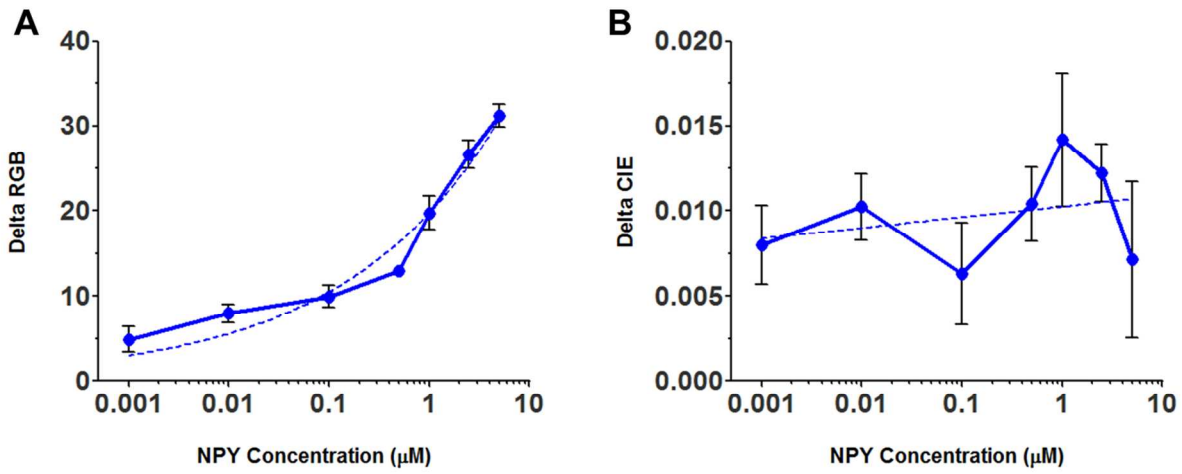

Figure 7. Comparison of Delta RGB and Delta CIE Image Change Quantification Methods for P-ELISA. (A) Delta RGB measurements from a digital image of a NPY P-ELISA. (B) Delta CIE measurements from the same digital image of the NPY P-ELISA. Error bars indicate SEM with n=4.

The program accomplishes this automation through a series of unique steps. First, the image is converted to a purely black and white image using a threshold value (Supplemental Figure 3B). Next, the white areas of the image are evaluated whether they are circular in nature and of sufficient pixel area to be a test spot, and their centroids are recorded for location in the image. From this information, an initial image mask is developed (Supplemental Figure 3C). To make sure the edges of the test zones are excluded due to the possibility of wax color being incorporated into the RGB averages, the radius of each white area on the mask is decreased by 50% and a new mask is made (Supplemental Figure 3D). The mask is applied to the original RGB image and the average RGB values for each white area of the mask are stored. The delta RGB values are calculated and input into the concentration correlation function to determine the

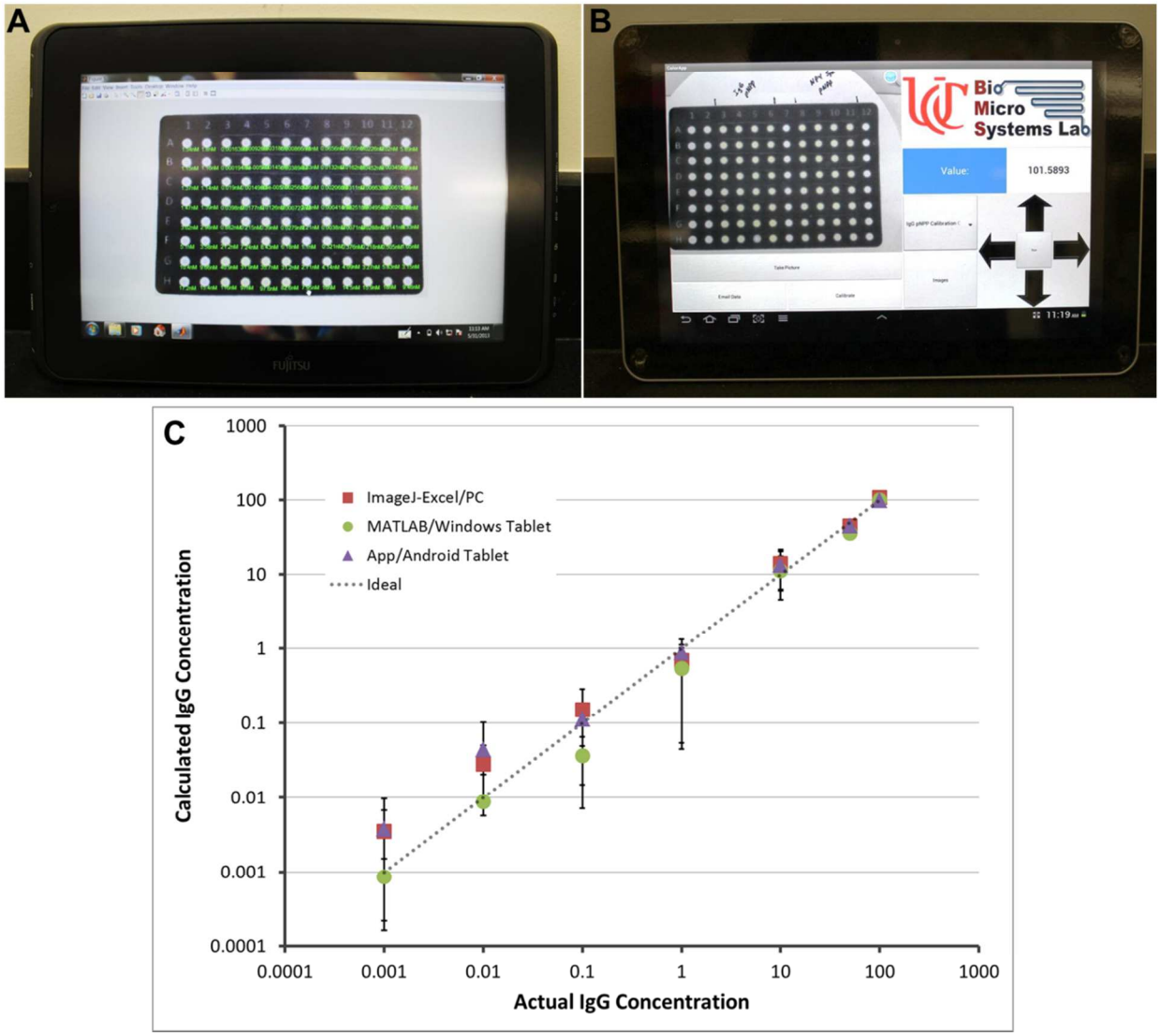

Figure 8. Image Analysis and Quantification of IgG P-ELISA Results with Windows- and Android-based Tablets. (A) Fujitsu Stylistic Q550 Tablet with Windows 7 running MATLAB for automated image analysis and quantification. (B) Samsung Galaxy Tab 10.1 (GT-P7510) with Android 4.0.4 running a custom designed App (.APK) for manual calibration and automated quantification. (C) Comparison of calculated IgG concentrations from the same IgG-pNPP P-ELISA via 3 different methods: 1) Manual image analysis using ImageJ-Excel on a PC, 2) Automated image analysis using MATLAB on a Windows tablet, and 3) Manual/automated image analysis using app on Android tablet. Error bars indicate SEM with n=4.

corresponding antigen concentration, which is displayed on the final output image (Supplemental Figures 3E and 4). The program is able to output all results as an Excel file as well.

While the correlation function must be predetermined and input into the program, we are currently working on incorporating a built-in calibration method as well as allowing for the program to automatically perform image correction for uneven lighting conditions across the test zones, as was presented in our earlier work[46]. Simply printing a simulated pNPP scale onto the paper for standardized calibration is not feasible since multiple factors in the P-ELISA (i.e. ambient temperature and humidity, freshness of substrates, etc.) affect the amount of enzyme substrate color production. Therefore, a standard dilution series of a positive control would most likely still need to be performed in parallel with any assay as is done with normal ELISAs.

For non-MATLAB capable platforms, we have developed an android-based application which can perform many of the same analysis features. The app allows a user to image a paper-based 96-well microplate, define a calibration series by selecting test zones and inputting the corresponding concentration, and then perform individual automated calculation of antigen levels in unknown samples (Figure 8B). The app performs concentration correlation through the same delta RGB calculations as performed for all experiments in this manuscript. However, since the system directly implements the regression algorithm, the main advantage is that the app can be further developed to evaluate different generalizations of linear regressions to determine which provides the best fits for the data when building a calibration curve. We are also working on incorporating the automated image analysis features described in the MATLAB version through implementation of Hough transform.

When comparing results from all three analysis methods, currently the automated MATLAB image analysis method most closely matches the calculated vs. actual concentration ratio, with an average difference of 24.9%, followed by the ImageJ-Excel method at 81.2% and the manual/automated Android app at 98.55% (Figure 8C). The correlation results of the Android app can most likely be improved through the use of the automated image processing, as in the MATLAB version, which would eliminate any user variability when selecting analysis areas as seen in the ImageJ-Excel method. Also, incorporating the lighting correction function should help reduce variability between columns of replicate samples with reference calibration points around each test area.

Conclusions

The ability to detect and monitor human performance biomarkers gives the potential to track an individual during a task and determine their physiological stress and cognitive load levels. In a military application, this could allow for field medics to asses a soldier's stress level to help prevent PTSD, allow a field medic to determine if a soldier has suffered a traumatic brain injury (TBI) and begin treatment immediately to prevent further damage, or allow assessment of vigilance for soldiers in non-battlefield positions where inattentiveness could lead to mission failure. Tracking NPY and other relevant biomarkers (i.e. Orexin A, Cortisol, Glutamate) could help to prevent these situations.

Wax-printed paper-based diagnostics provide a unique and inexpensive platform to carry out biomolecular assays at very low sample and reagent volumes. Paper-based ELISAs were shown here to have pM to nM sensitivity using colorimetric substrates, even in a complex

sample such as saliva, but could be enhanced further with assay optimization, use of alternate enzyme substrates, or nanoparticle-based enzyme-free assays. Additionally, the cost and time savings of performing a P-ELISA instead of a conventional ELISA would significantly increase not only the number of samples per dollar the laboratory would be able to process, but the number of patients in the same time period as well. The ability to use a smartphone or tablet platform to perform quick analysis of paper-based diagnostics can provide an easier alternative to expensive, time consuming laboratory procedures. This technology could be extremely beneficial in resource-limited laboratory environments, where diagnostic measurement equipment, such as spectrophotometers or multi-well plate readers, is not easily obtained due to funding constraints.

Acknowledgements

This work was supported by the Air Force Research Laboratory, 711th Human Performance Wing, Human Signatures Branch. We are grateful to Dr. Dan Powers and Maj. Monika Lunn for their technical guidance and support during this effort, as well as the Molecular Signatures Section team members.

References

1. Langan-Fox, J.; Sankey, M. J.; Canty, J. M. *Hum. Factors* **2009** *51*, 595-637.
2. Weinger, M. B. *J.Clin. Monit. Comput.* **1999** *15*, 549-552.
3. Buchheit, M.; Simpson, M. B.; Al Haddad, H.; Bourdon, P. C.; Mendez-Villanueva, A. *Eur. J. Appl. Physiol.* **2012** *112*, 711-723.
4. Weinger, M. B. *J.Clin. Monit. Comput.* **1999** *15*, 319-323.
5. Grose, V. L. *Professional Safety* **1989** *34*, 24-26.
6. O'Hanlon, J. F. *Acta Psychol. (Amst)* **1981** *49*, 53-82.
7. Cummings, M. L.; Mastracchio, C.; Thornburg, K. M.; Mkrtchyan, A. *Interact. Comput*. **2013** *25*, 34-47.
8. Morgan, C. A.; Wang, S.; Southwick, S. M.; Rasmusson, A.; Hazlett, G.; Hauger, R. L.; Charney, D. S. *Biol. Psychiatry* **2000** *47*, 902-909.
9. Eaton, K.; Sallee, F. R.; Sah, R. *Curr. Top. Med. Chem.* **2007** *7*, 1645-1659.
10. Heilig, M. *Neuropeptides* **2004** *38*, 213-224.
11. Redrobe, J. P.; Dumont, Y.; Herzog, H.; Quirion, R. *J. Mol. Neurosci*. **2004** *22*, 159-166.
12. Redrobe, J. P.; Dumont, Y.; St-Pierre, J. A.; Quirion, R. *Brain research*, **1999** *848*, 153-166.
13. Chen, X.; Henderson, K.; Beinfeld, M. C.; Westfall, T. C. *J. Cardiovasc. Pharmacol*. **1988** *12*, 473-478.
14. Martin, J. R.; Knuepfer, M. M.; Beinfeld, M. C.; Westfall, T. C. *Am. J. Physiol. Heart Circ. Physiol.* **1989** *257*, H791-H798.
15. Clark, J. T.; Kalra, P. S.; Crowley, W. R.; Kalra, S. P. *Endocrinology* **1984** *115*, 427-429.
16. Zukowska-Grojec, Z. *Ann. N. Y. Acad. Sci*. **1995** *771*, 219-233.
17. Sah, R.; Geracioti, T. D. *Mol. Psychiatry* **2012** *18*, 646-655.
18. Adrian, T. E.; Allen, J. M.; Bloom, S. R.; Ghatei, M. A.; Rossor, M. N.; Roberts, G. W.; Crow, T. J.; Tatemoto, K.; Polak, J. M. *Nature* **1983** *306*, 584 – 586.
19. Allen, Y. S.; Adrian, T. E.; Allen, J. M.; Tatemoto, K.; Crow, T. J.; Bloom, S. R.; Polak, J. M. *Science* **1983** *221*, 877-879.
20. Lundberg, J. M.; Hökfelt, T. *Prog. Brain Res.* **1986** *68*, 241-262.
21. Morgan, C. A.; Wang, S.; Rasmusson, A.; Hazlett, G.; Anderson, G.; Charney, D. S. *Psychosom. Med.* **2001** *63*, 412-422.
22. Duan, H.; Hao, C.; Fan, Y.; Wang, H.; Liu, Y.; Hao, J.; Xu, C.; Liu, X.; Zhang, H. *J. Surg. Res.* **2013** *184*, 1006-1012.
23. Martinez, A. W.; Phillips, S. T.; Butte, M. J.; Whitesides, G. M. *Angew. Chem. Int. Ed.* **2007** *46*, 1318-1320.
24. Bruzewicz, D. A.; Reches, M.; Whitesides, G. M. *Anal. Chem*. **2008** *80*, 3387-3392.
25. Wang, S.; Xu, F.; Demirci, U. *Biotechnol. Adv.* **2010** *28*, 770-781.
26. Alyassin, M. A.; Moon, S.; Keles, H. O.; Manzur, F.; Lin, R. L.; Hæggstrom, E.; Kuritzkes, D.R.; Demirci, U. (2009). Rapid automated cell quantification on HIV microfluidic devices. *Lab Chip* **2009** *9*, 3364-3369.

27. Cheng, C. M.; Martinez, A. W.; Gong, J.; Mace, C. R.; Phillips, S. T.; Carrilho, E.; Mirica, K. A.; Whitesides, G. M. *Angew. Chem. Int. Ed.* **2010** *49*, 4771-4774.
28. Wang, S.; Ge, L.; Song, X.; Yu, J.; Ge, S.; Huang, J.; Zeng, F. *Biosens. Bioelectron.* **2012** *31*, 212-218.
29. Martinez, A. W. *Bioanalysis* **2011** *3*, 2589-2592.
30. Wang, W.; Wu, W. Y.; Zhu, J. J. *J. Chromatogr. A* **2010** *1217*, 3896-3899.
31. Lee, D. S.; Jeon, B. G.; Ihm, C.; Park, J. K.; Jung, M. Y. *Lab Chip* **2011** *11*, 120-126.
32. Nash, M. A.; Hoffman, J. M.; Stevens, D. Y.; Hoffman, A. S.; Stayton, P. S.; Yager, P. *Lab* Chip **2010** *10*, 2279-2282.
33. Lee, W. G.; Kim, Y. G.; Chung, B. G.; Demirci, U.; Khademhosseini, A. *Adv. Drug Delivery Rev.* **2010** *62*, 449–457.
34. Yager, P.; Edwards, T.; Fu, E.; Helton, K.; Nelson, K.; Tam, M. R.; Weigl, B. H. *Nature* **2006** *442*, 412–418.
35. Martinez, A. W.; Phillips, S. T.; Whitesides, G. M.; Carrilho, E. *Anal. Chem.* **2010** *82*, 3–10.
36. Carrilho, E.; Phillips, S. T.; Vella, S. J.; Martinez, A. W.; Whitesides, G. M. *Anal. Chem.* **2009** *81*, 5990 – 5998.
37. Yu, L.; Li, C. M.; Liu, Y.; Gao, J.; Wang, W.; Gan, Y. *Lab Chip* **2009** *9*, 1243–1247.
38. Tohda, K.; Gratzl, M. *Anal. Sci.* **2006** *22*, 383–388.
39. Suzuki, K.; Hirayama, E.; Sugiyama, T.; Yasuda, K.; Okabe, H.; Citterio, D. *Anal. Chem.* **2002** *74*, 5766–5773.
40. Soldat, D. J.; Barak, P.; Lepore, B. J. *J. Chem. Educ.* **2009** *86*, 617–620.
41. DiScipio, R. G. *Anal. Biochem*. **1996** *236*, 168–170.
42. Obare, S. O.; Hollowell, R. E.; Murphy, C. J. *Langmuir* **2002** *18*, 10407–10410.
43. Tom, R. T.; Suryanarayanan, V.; Reddy, P. G.; Baskaran, S.; Pradeep, T. *Langmuir* **2004** *20*, 1909–1914.
44. Ji, X.; Song, X.; Li, J.; Bai, Y.; Yang, W.; Peng, X. *J. Am. Chem. Soc.* **2007** *129*, 13939-13948.
45. Shen, L.; Hagen, J. A.; Papautsky, I. *Lab Chip* **2012** *12*, 4240-4243.
46. Dawidson, I.; Blom, M.; Lundeberg, T.; Theodorsson, E.; Angmar-Månsson, B. *Life Sci.* **1996** *60*, 269-278.

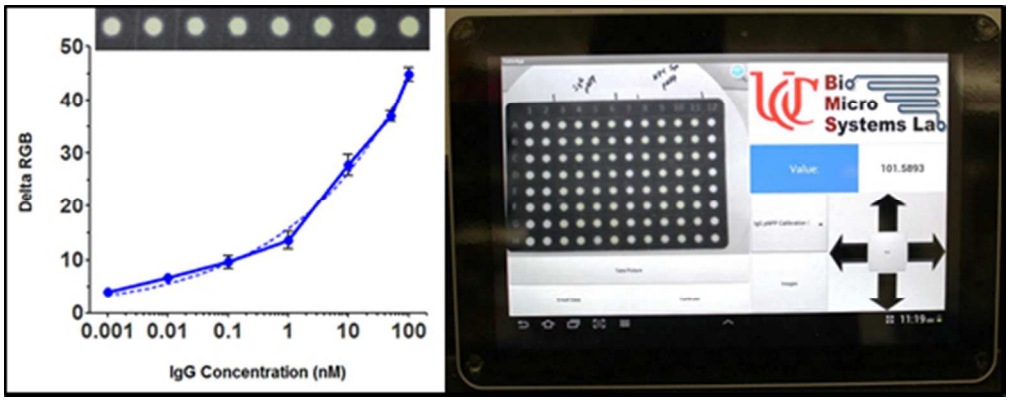

90x35mm (150 x 150 DPI)